Electronic Supplementary Material (ESI) for Journal of Materials Chemistry A.

Highly Oriented Conductive MOF Thin Film Based Schottky Diode for Self-Powered Light and Gas Detection

Lin-An Cao, Ming-Shui Yao, Hui-Jie Jiang, Susumu Kitagawa, Xiao-Liang Ye, Wen-Hua Li and Gang Xu*

Computational formulas

According to the thermionic emission theory model, the nonlinear *I-V* characteristic of Schottky diode is given by the following equation:[1]

$I = I_0\ [exp\ (\frac{eV}{\eta k_B T})\ -1]$, where I is current across the diode, V is applied voltage, T is absolute temperature, k_B is the Boltzmann's constant, η is the ideality factor which can be expressed as $\eta = (\frac{e}{k_B T})\ (\frac{dV}{dlnI})$. I_0 is reversed saturated current and can be described by following equation : $I_0 = A^*T^2\ exp\ (-\frac{e\Phi_B}{k_B T})$, where A^* is the effective Richardson constant ($\approx$ 252 A K^{-2} for n-type silicon)[2] and Φ_B is the zero-bias and Φ_B is the zero-bias Schottky-barrier height. Φ_B can be calculated from short-circuit current. Figure S13 are semi-logarithm plots of current-voltage curves for Ag/n-Si/Al and Ag/$M_3(C_{18}H_6X_6)_2$/n-Si/Al. The large short-circuit current in Ag/n-Si mainly results from lower Schottky barrier height between silver electrode and n-type silicon. After EC-MOFs thin film insertion, short-circuit current significantly decreases from 10^{-5} A for Ag/n-Si to 10^{-10} A for Ag/$Cu_3(C_{18}H_6O_6)_2$/n-Si. The series resistance R_S can be extracted by the following equation: [3]

$$\frac{dV}{dlnI} = \frac{\eta k_B T}{e} + R_S I.$$

Computational formulas for photodetector parameters:

Responsitivity $R_\lambda = \frac{I_{photo}}{PS}$, where I_{photo} is the photocurrent at zero voltage, P is incident light intensity, S is active device area.

External quantum efficiency EQE $= \frac{hcR_\lambda}{e\lambda}$, where h, c and e are Plank constant, speed of light and charge of electron, respectively.

Detectivity $D^* = \frac{\sqrt{S}R_\lambda}{\sqrt{2eI_{dark}}}$, where I_{dark} is the dark current at zero voltage.

The rise and fall time can also be obtained which determined from the time interval for the photocurrent rising (decaying) from 10% (90%) to 90% (10%) of its peak value, respectively.

Impedance Spectroscopy Measurement

The impedance spectroscopy measurement was measured over the range of 1 Hz to 1 MHz with an oscillation amplitude of 10 mV and 0 V DC under 450 nm light illumination. The impedance spectroscopy of Ag/$Cu_3(C_{18}H_6(NH)_6)_2$/n-Si/Al device and fitted equivalent circuit are shown in Figure S15. R_1, R_2 and C_1 are series resistance, recombination resistance and the chemical capacitance, respectively. The carrier lifetime is the product of R_2 and C_1.[17] Carrier lifetime of Ag/$Cu_3(C_{18}H_6(NH)_6)_2$/n-Si/Al device is 0.12 μs at 450 nm light illumination. Carrier diffusion length (L_D) determined by $L_D = (k_B\, T\, \mu\, \tau_r/e)^{1/2}$ is 27.3 nm in the $Cu_3(C_{18}H_6(NH)_6)_2$ film, where k_B, T, μ, τ_r and e are the Boltzmann constant, temperature, carrier mobility, carrier lifetime and elementary charge, respectively.[4] The carrier mobility of $Cu_3(C_{18}H_6(NH)_6)_2$ film is 0.02 $cm^2/V/s$ according to Hall measurement.

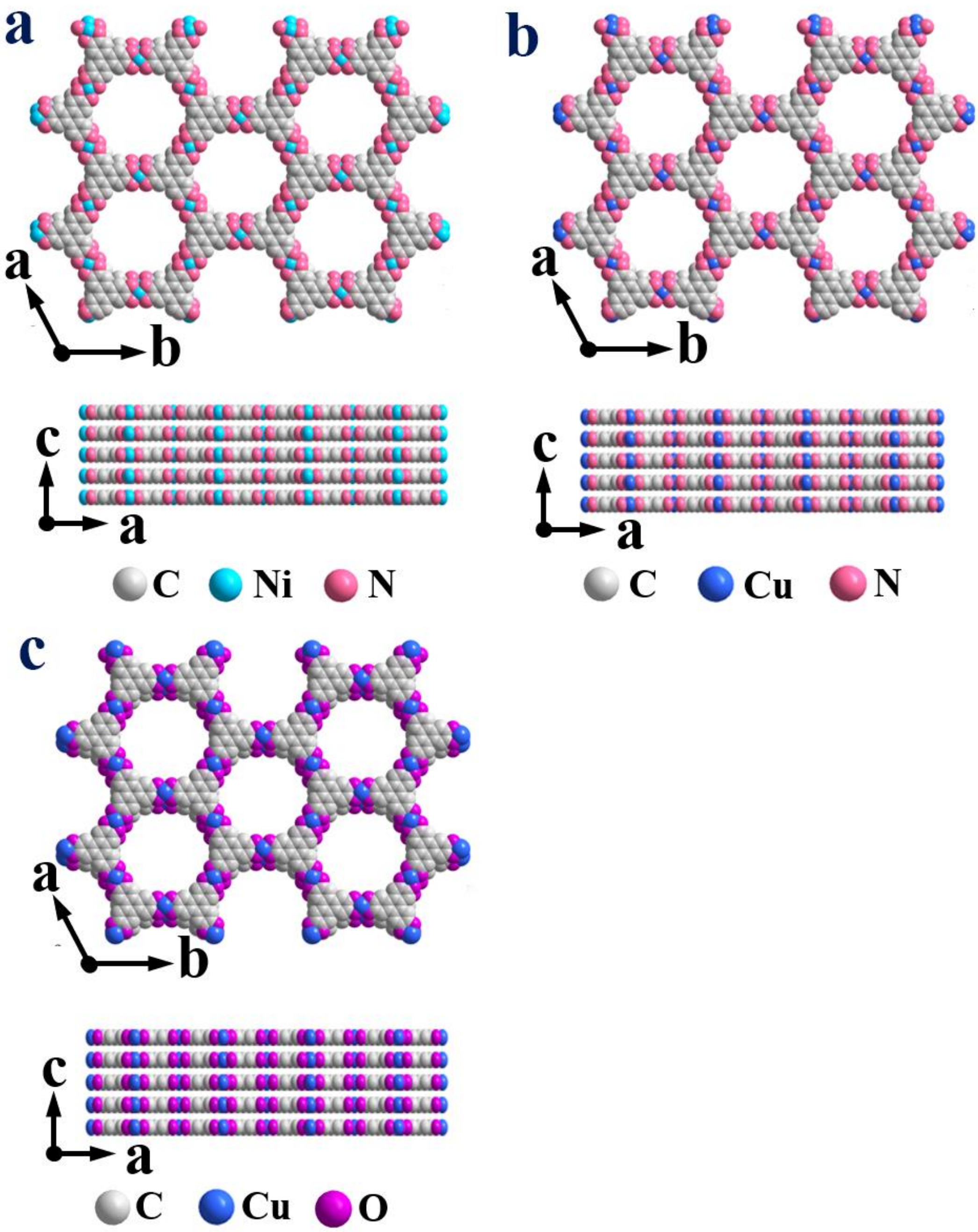

Figure S1. Crystalline structure of (a) $Ni_3(C_{18}H_6(NH)_6)_2$; (b) $Cu_3(C_{18}H_6(NH)_6)_2$ and (c) $Cu_3(C_{18}H_6O_6)_2$.

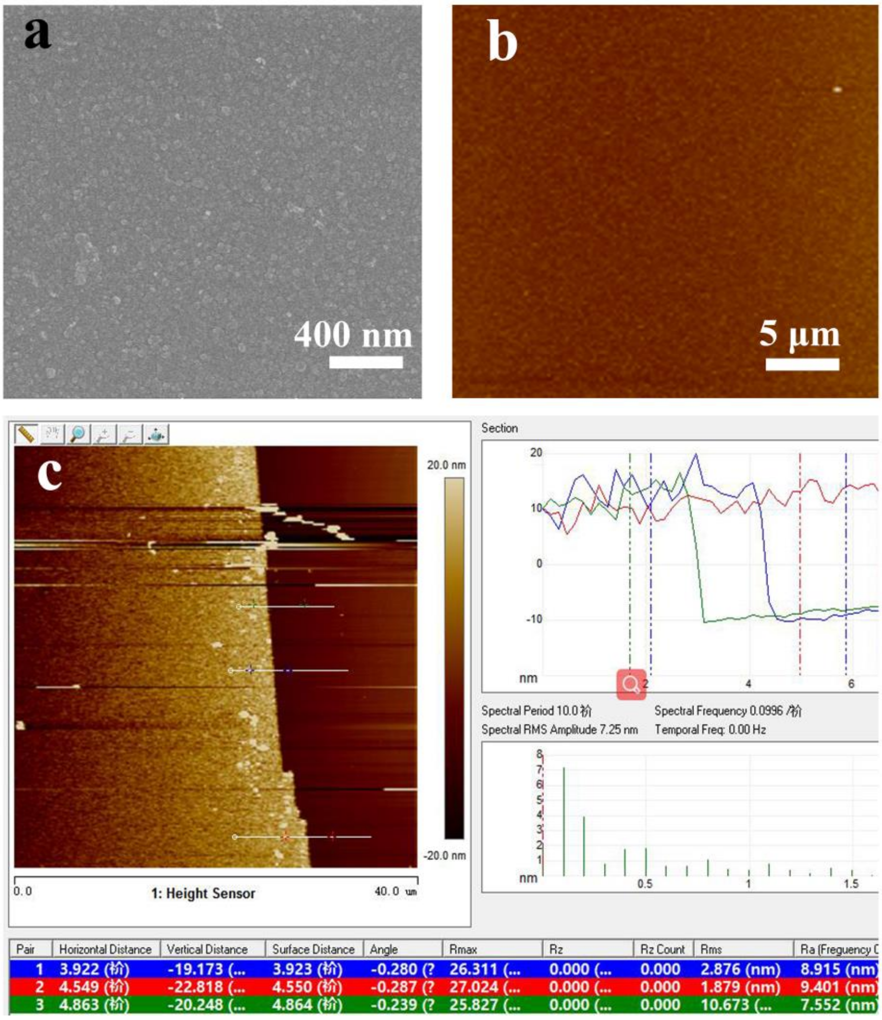

Figure S2. (a) Top views HR-SEM; (b) Top view AFM image; (c) AFM image of the edge of $Cu_3(C_{18}H_6O_6)_2$-20nm thin film.

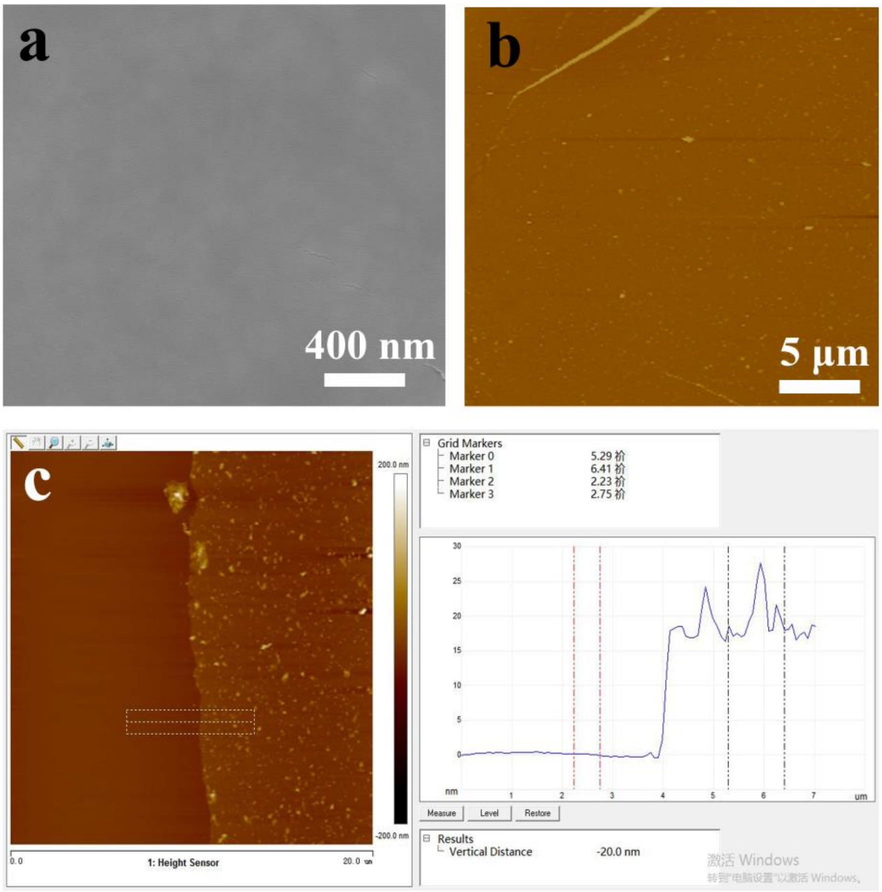

Figure S3. (a) Top views HR-SEM; (b) Top view AFM image; (c) AFM image of the edge of $Ni_3(C_{18}H_6(NH)_6)_2$-20nm thin film.

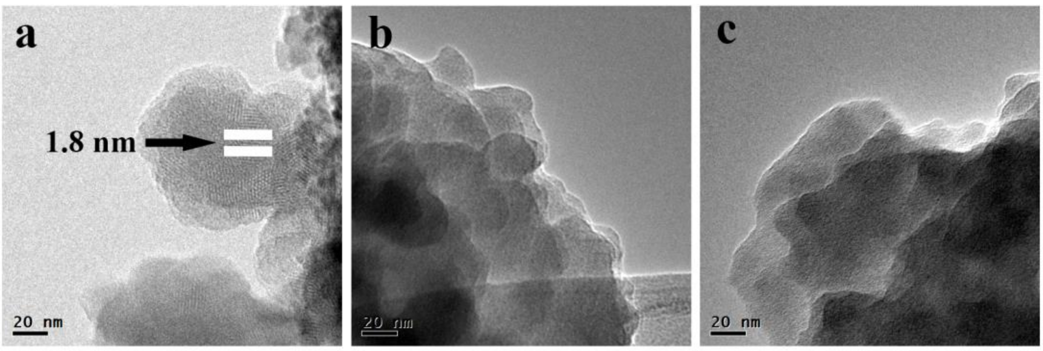

Figure S4. HR-TEM images of (a) $Ni_3(C_{18}H_6(NH)_6)_2$, (b) $Cu_3(C_{18}H_6(NH)_6)_2$ and (c) $Cu_3(C_{18}H_6O_6)_2$, respectively.

$Ni_3(C_{18}H_6(NH)_6)_2$ thin film possess obvious lattice fringes with lattice spacing of 1.8 nm which is consistent with the periodic arrangement of HITP interconnected by nickel center. $Cu_3(C_{18}H_6(NH)_6)_2$ and $Cu_3(C_{18}H_6O_6)_2$ thin film prepared by layer-by-layer method are distinct lamellar film.

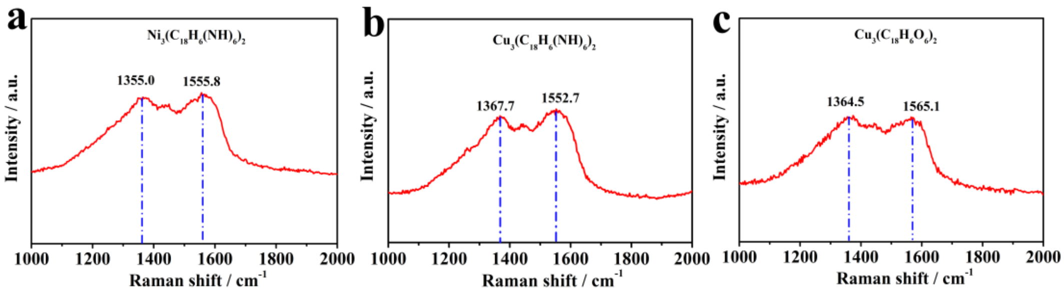

Figure S5. Raman spectra of (a) $Ni_3(C_{18}H_6(NH)_6)_2$, (b) $Cu_3(C_{18}H_6(NH)_6)_2$ and (c) $Cu_3(C_{18}H_6O_6)_2$ film.

Raman characterization revealed three peaks at about 1355.0, 1367.7 and 1364.5 cm^{-1} in $Ni_3(C_{18}H_6(NH)_6)_2$, $Cu_3(C_{18}H_6(NH)_6)_2$ and $Cu_3(C_{18}H_6O_6)_2$, respectively, reminiscent of the D bands of 2D graphitic materials. Correspondingly, other three peaks at about 1555.8, 1552.7 and 1565.1 cm^{-1} in $Ni_3(C_{18}H_6(NH)_6)_2$, $Cu_3(C_{18}H_6(NH)_6)_2$ and $Cu_3(C_{18}H_6O_6)_2$, respectively, reminiscent of the G bands of 2D graphitic materials.[5]

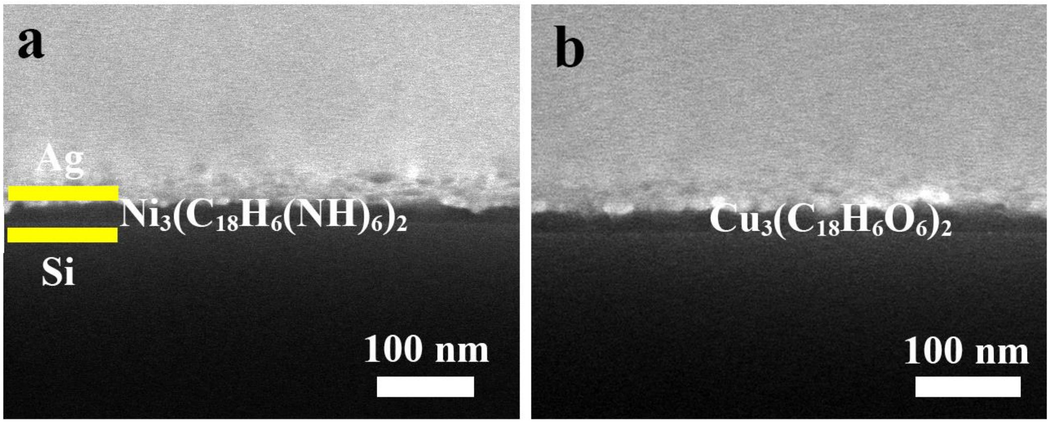

Figure S6. HR-SEM cross-section views of (a) Ag/$Ni_3(C_{18}H_6(NH)_6)_2$-20nm /n-Si; (b) Ag/$Cu_3(C_{18}H_6O_6)_2$-20nm /n-Si device.

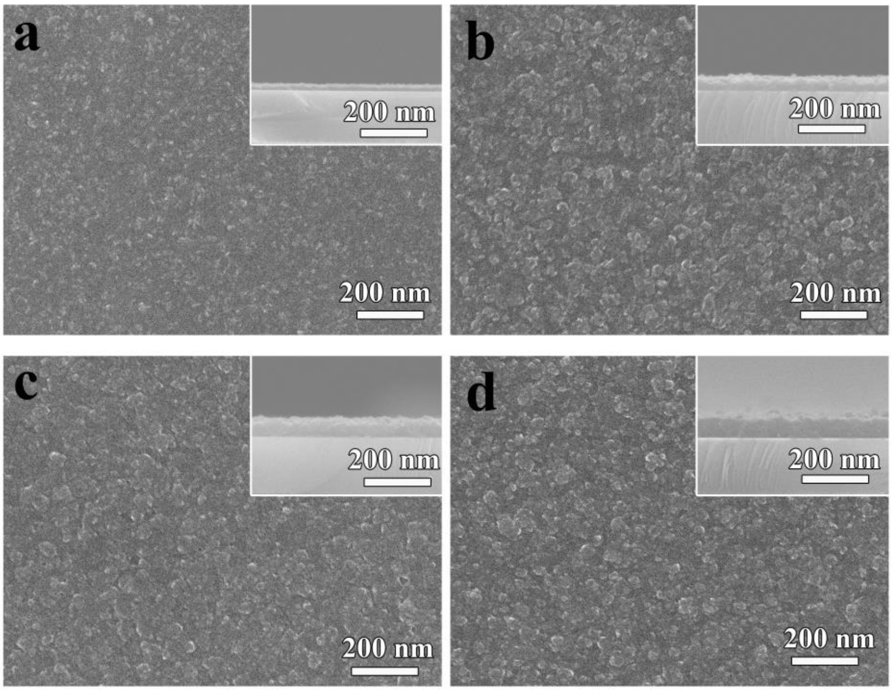

Figure S7. Top views HR-SEM of $Cu_3(C_{18}H_6(NH)_6)_2$-xnm thin film in which x are (a) 40; (b) 60; (c) 80 and (d) 100 (insets are cross sectional views).

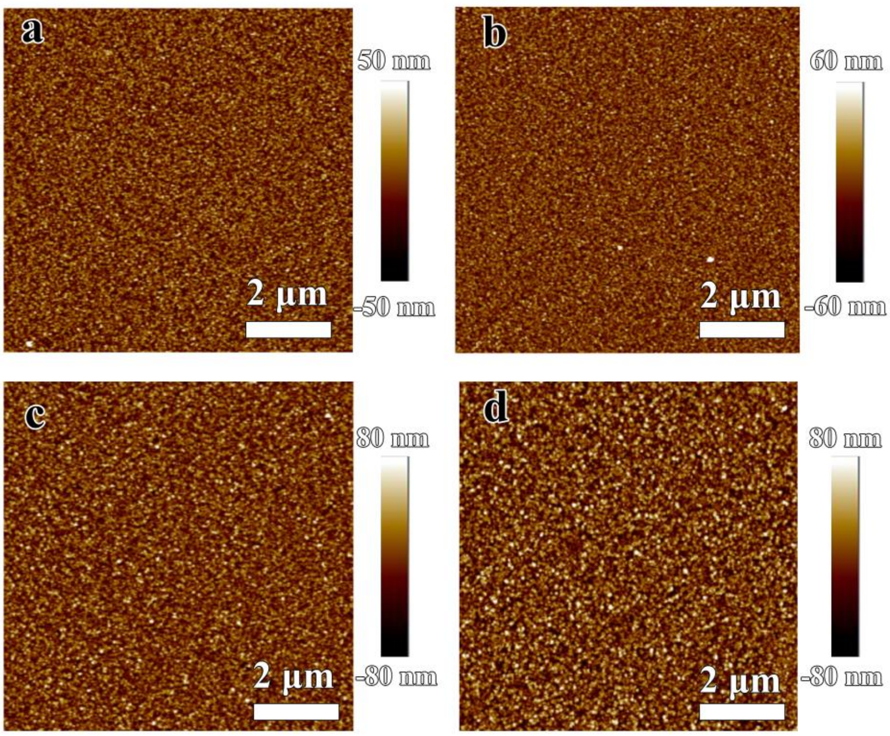

Figure S8. Top view AFM images of $Cu_3(C_{18}H_6(NH)_6)_2$-xnm thin film in which x are (a) 40; (b) 60; (c) 80 and (d) 100, respectively.

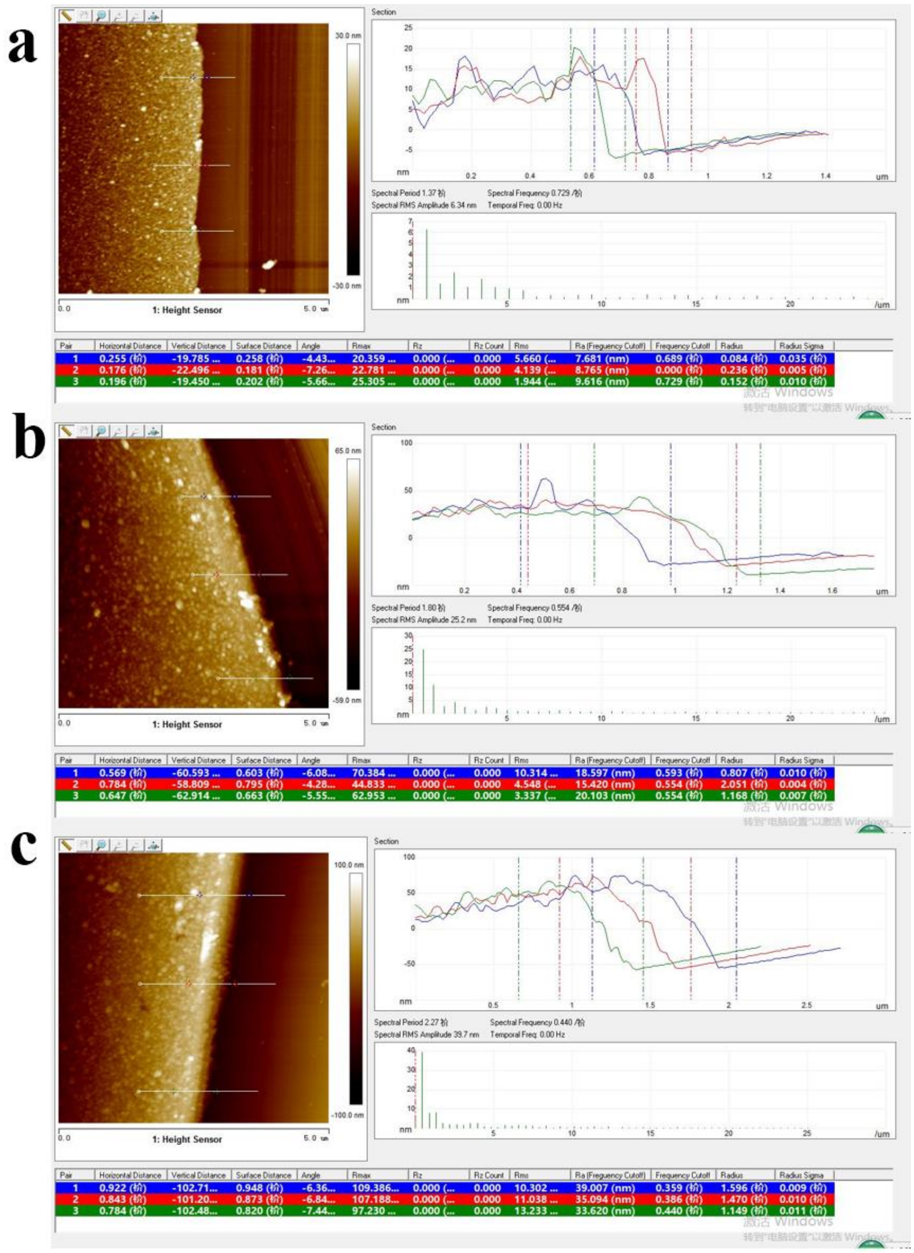

Figure S9. AFM images of the edge of $Cu_3(C_{18}H_6(NH)_6)_2$-xnm thin film with (a) 20nm; (b) 60nm and (c)100nm, respectively.

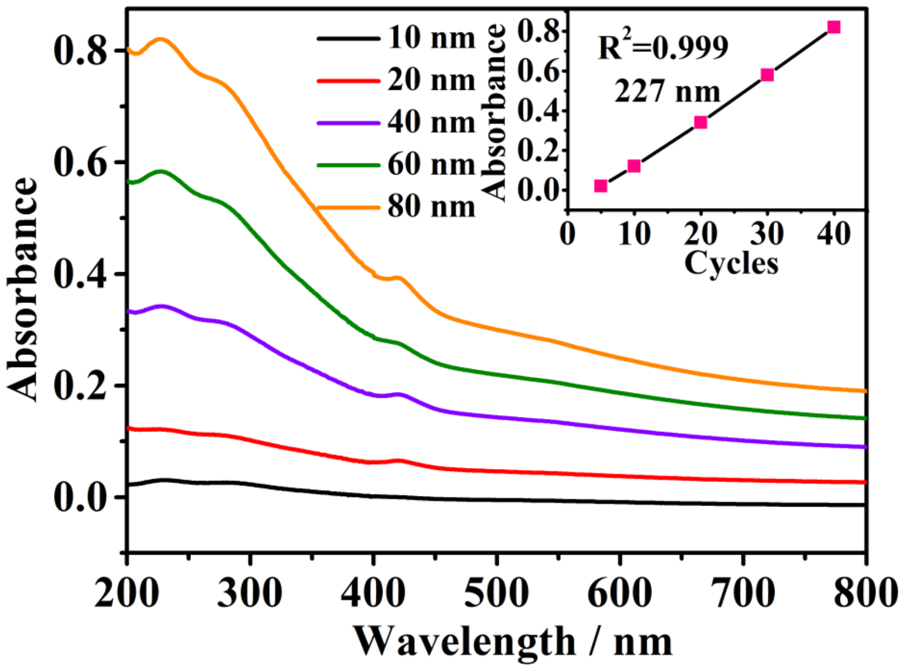

Figure S10. UV-Vis absorbance spectra of $Cu_3(C_{18}H_6(NH)_6)_2$-xnm (inset is cycle-dependent intensity of absorbance at 227 nm.

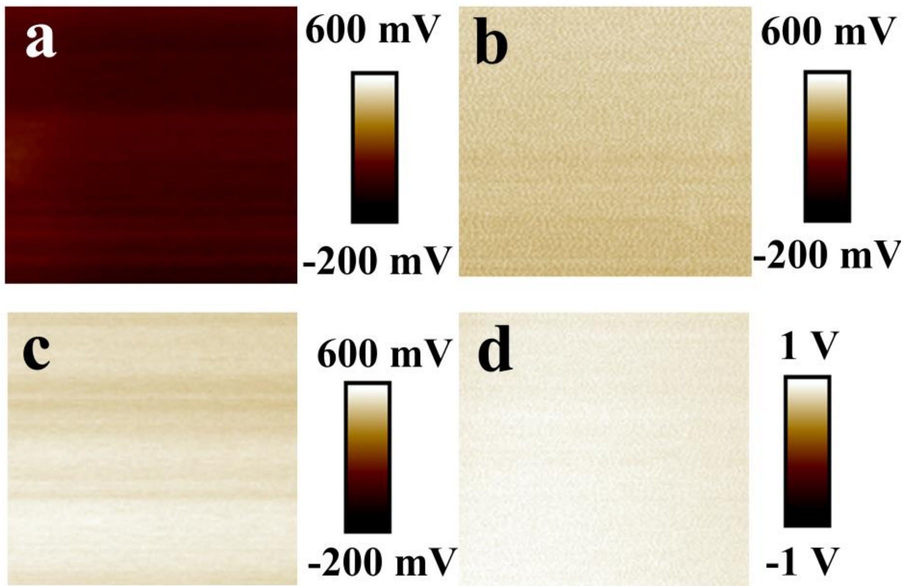

Figure S11. KPFM patterns of (a)Ag; (b) $Ni_3(C_{18}H_6(NH)_6)_2$-20nm; (c) $Cu_3(C_{18}H_6(NH)_6)_2$-20nm and (d) $Cu_3(C_{18}H_6O_6)_2$-20nm thin film.

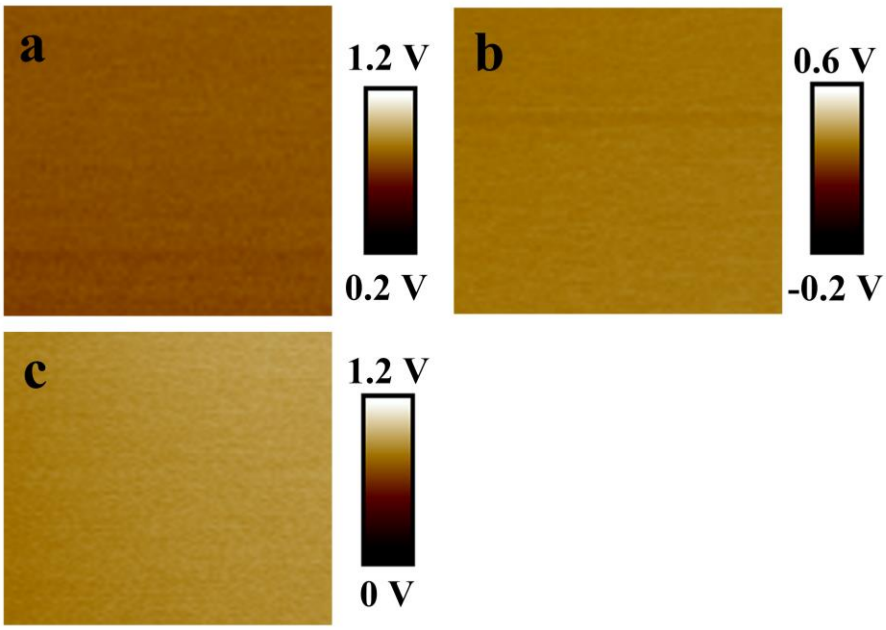

Figure S12. KPFM of (a) $Ag/Ni_3(C_{18}H_6(NH)_6)_2$-20nm; (b) $Ag/Cu_3(C_{18}H_6(NH)_6)_2$-20nm and (c) $Ag/Cu_3(C_{18}H_6O_6)_2$-20nm.

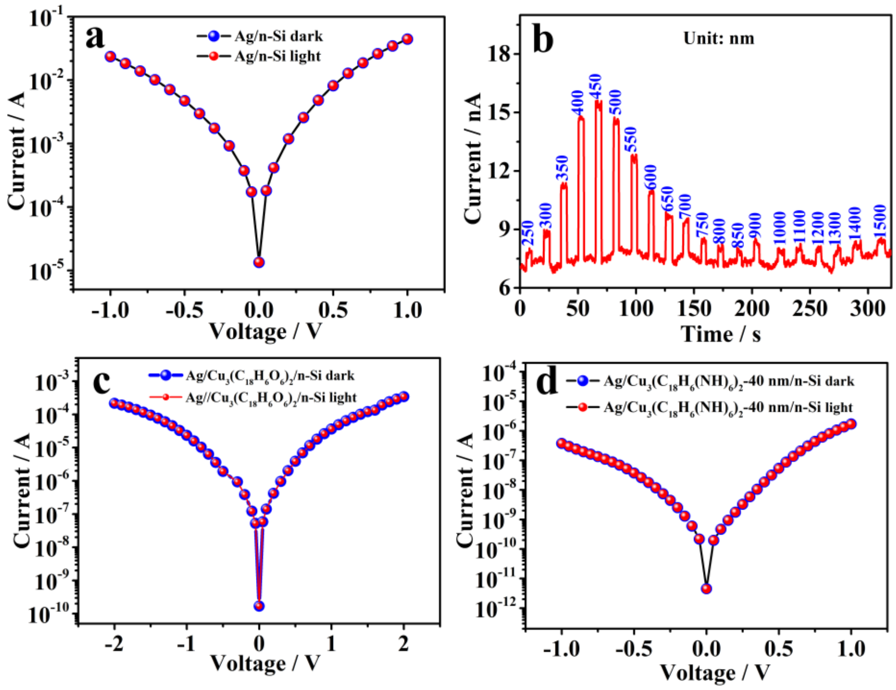

Figure S13. (a) Semi-logarithm plot of current-voltage for Ag/n-Si/Al under illumination and dark condition; (b) Time-dependent photoresponse of $Ag/Ni_3(C_{18}H_6(NH)_6)_2$/n-Si under different wavelength light; (c) Semi-logarithm plot of current-voltage for $Ag/Cu_3(C_{18}H_6O_6)_2$/n-Si under illumination and dark condition; (d) Semi-logarithm plot of current-voltage for $Ag/Cu_3(C_{18}H_6(NH)_6)_2$-40nm/n-Si under illumination and dark condition.

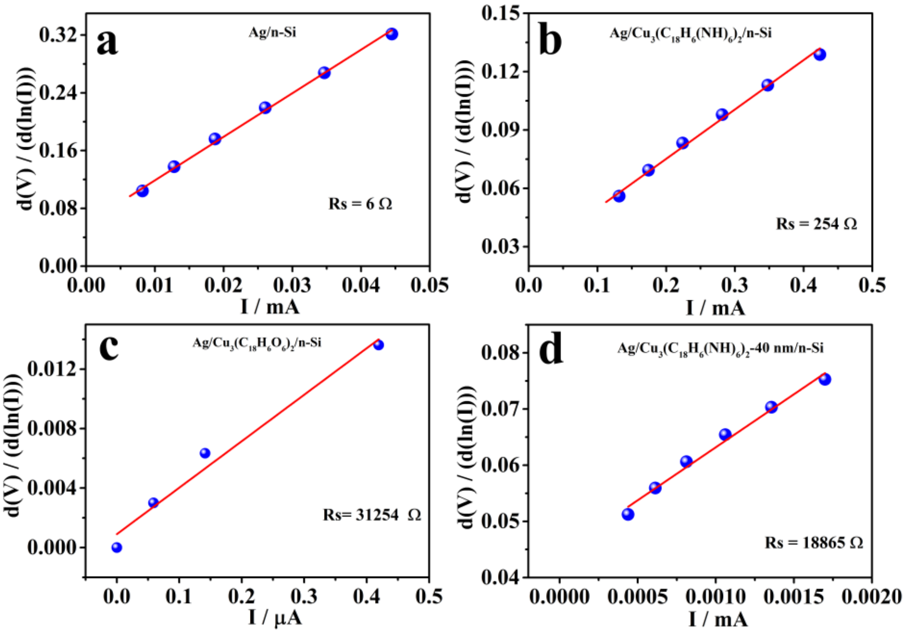

Figure S14. dV/dlnI versus I plot of (a) Ag/n-Si, (b) Ag/$Cu_3(C_{18}H_6(NH)_6)_2$/n-Si; (c) Ag/$Ni_3(C_{18}H_6O_6)_2$/n-Si and (d) Ag/$Cu_3(C_{18}H_6(NH)_6)_2$-40nm/n-Si, respectively.

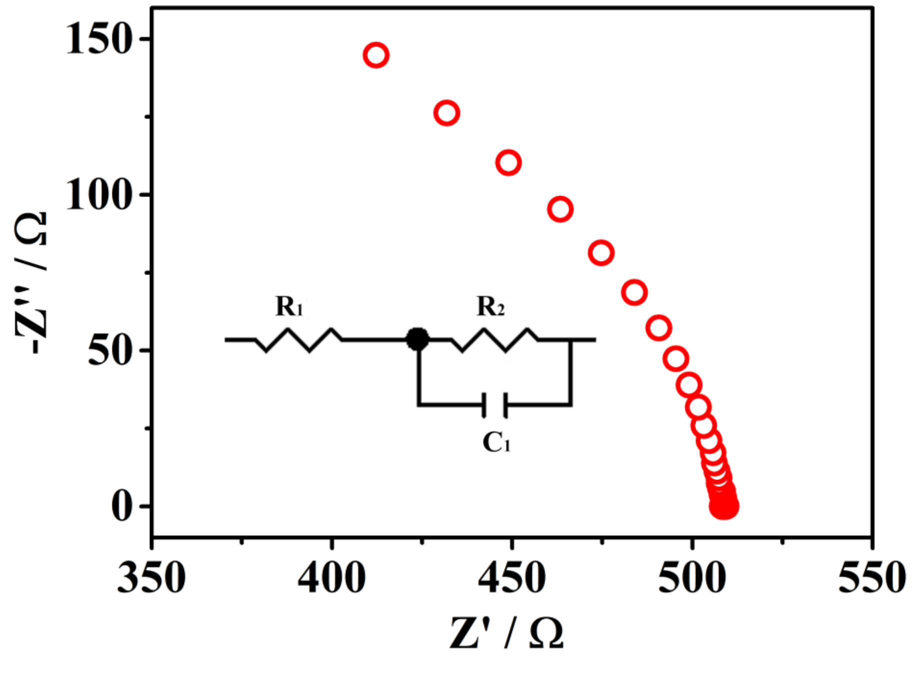

Figure S15. Impedance spectroscopies of Ag/$Cu_3(C_{18}H_6(NH)_6)_2$/n-Si/Al under 450nm light illumination (inset is fitted equivalent circuit).

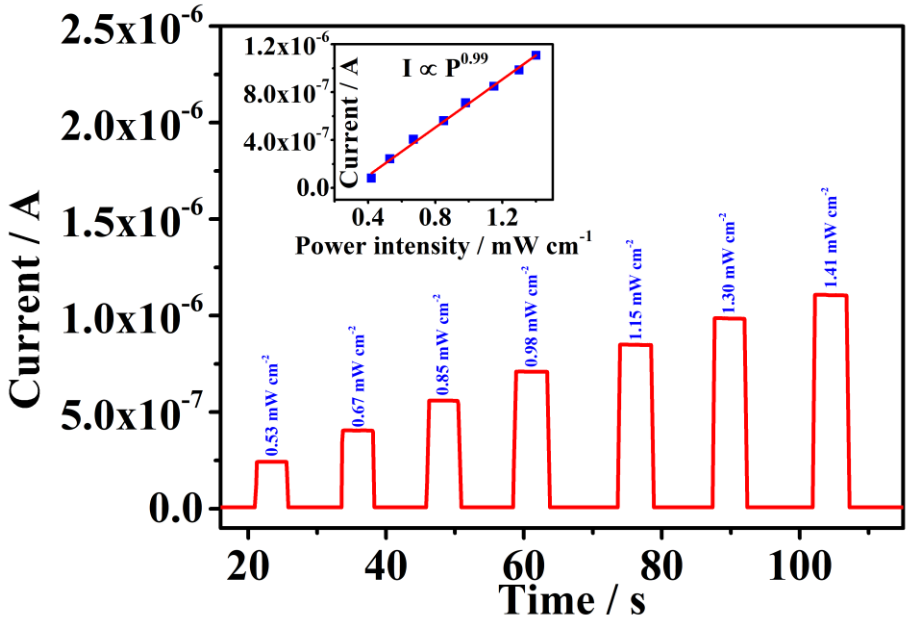

Figure S16. Photo response of Ag/$Cu_3(C_{18}H_6(NH)_6)_2$/n-Si under 450nm light illumination with different intensity, the inset shows the photocurrent variation with light intensity fitted by power law.

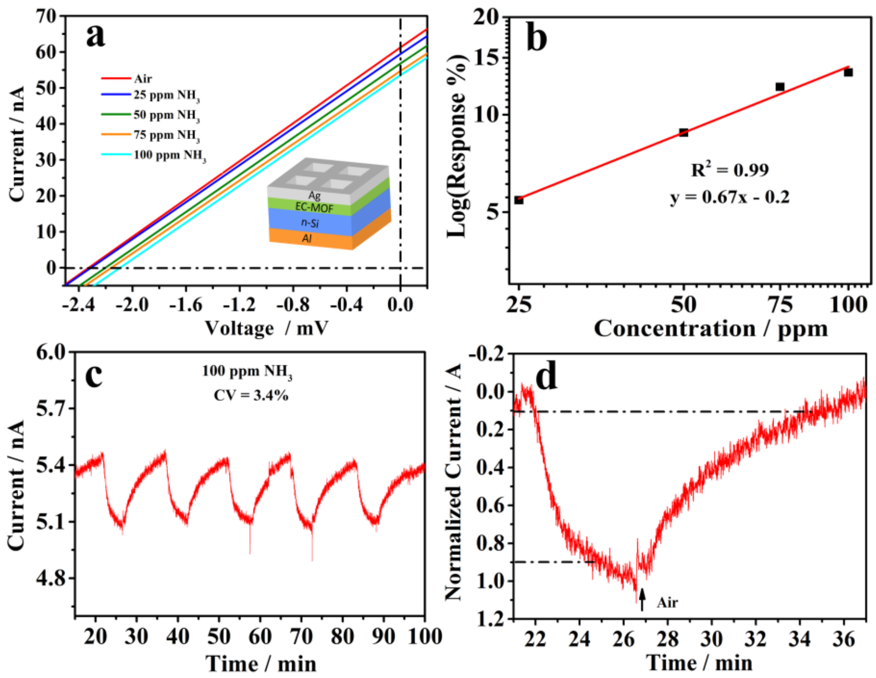

Figure S17. (a) Partial current-voltage characteristics of Ag/$Cu_3(C_{18}H_6(NH)_6)_2$/n-Si/Al diode in air and NH_3 atmosphere irradiating with 450nm visible light; (b) Linear fitted log-log plots of response and NH_3 concentration for Ag/$Cu_3(C_{18}H_6(NH)_6)_2$/n-Si/Al; (c) Five cycles response-recovery curves of Ag/$Cu_3(C_{18}H_6(NH)_6)_2$/n-Si/Al toward 100ppm NH_3; (d) Normalized response-recovery curves of Ag/$Cu_3(C_{18}H_6(NH)_6)_2$/n-Si/Al to 100ppm NH_3.

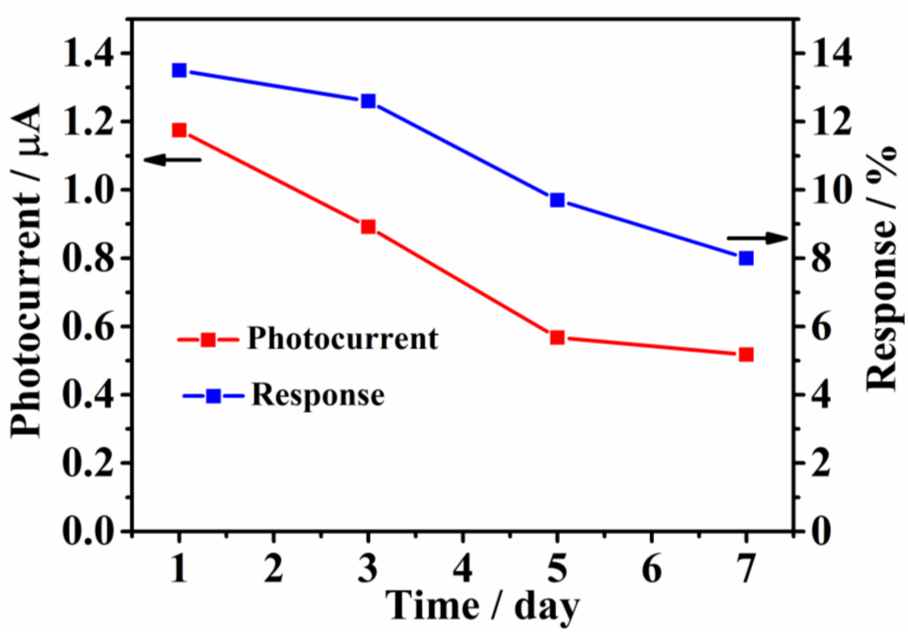

Figure S18. Long-term stability of $Ag/Cu_3(C_{18}H_6(NH)_6)_2$/n-Si for 7 days.

Table S1. Comparison of the key parameters for self-powered photoconductor

Materials	Device type	On/off ratio	Responsivity [mA W^{-1}]	Detectivity [Jones]	Rise/fall time	Response range (nm)	EQE (%)	Ref.
MoS_2/h-BN/graphene	vander waals	10^3	360	6.7×10^{10}		532	80	1[6]
MoS_2/p-Si	heterojunction	10^3	253	10^9	84/136 ms	532		2[7]
PEDOT:PSS/Si	heterojunction	10^5	37.8	4.1×10^{11}	2/172 μs	300-1100	80	3[8]
α-C/Si	heterojunction	10^2	292.5	2.9×10^{13}	8.3/33.1 μs	300-1100		4[9]
GaN//Si	heterojunction	10^4	210	7.5×10^{12}	9/8 ms	325-825	50	5[10]
Perovskite/TiO_2/Si	heterojunction	11^6		6×10^{12}	50/150 ms	350-1150		6[11]
Te/TiO_2	heterojunction	100	84	3.7×10^9	0.77/1.49 s	300-500		7[12]
PEDOT:PSS/P-TPD/QDs/ZnO	heterojunction	10^6	45	2.6×10^{12}	40 ms	300-900		8[13]
p-Si/n-CdS	p-n junction		5.9	1.3×10^{12}	245/277 μs	325-1550		9[14]
Pd-MoS_2/Si	p–n junction	10^2	654	10^{14}	2.1/173.8 μs	300-1100	35	10[15]
n-Si/p-NiO	p–n junction	10^2	430	1.5×10^{10}	<30 ms)	350–600	20	11[16]
Ag-p-NiO/n-rGO	p–n junction	10^3	72	3.95×10^{12}	0.80/0.84 s	365	24.5	12[17]
ZnO−Al_2O_3−Co_3O_4	p-i-n junction	≈4	21.8	4.12×10^{12}	6 s	vis		13[18]
Si/TiO_2/P_3HT	p-i-n junction	10^4	590(920)	1.38×10^{14}	84/153 μs	300-1100		14[19]
Graphene/ZnO/Si	Schottky	10^4	500		280/540 μs	400-1000		15[20]
Graphene/GaAs	Schottky		1.54		71/194 μs	532		16[1]
Graphene/MoO_3/Si	Schottky	≈10	400	5.4×10^{12}		300-1100	80	17[2]
(P3HT)/MoO_3/Ag	Schottky	10^4		6.03×10^{12}	26.9 μs	300-800	6.6	18[21]
CdS:Ga /Au	Schottky	10^3	8000		95/290 μs	350-650		19[22]
SiNWs/Cu	Schottky	10^4	335	2.9×10^{12}	3.6/14 μs	460-1100		20[23]
SiNWs/Ag NWs(5V)	Schottky	5			0.43/0.58 ms	400-1000		21[24]
Cu/p-Si	Schottky	≈10				White light		22[25]
Au/SnO_2 NW	Schottky	6.08	0.36 (370)	3.02×10^9	0.72/1.78 s	300-600		23[26]
Au-Si-Ti	Schottky		80			400-1000	10.3	24[27]
TiO_2/Ag NWs	Schottky	1700	32.5	6×10^9	44 ns/1.9 μs	200-400	16	25[28]
Ag/MOF/Si	Schottky	10^3	300	3.2×10^{11}	7/30 ms	250-1500	84	This work

Reference

1. Y. Wu, X. Yan, X. Zhang and X. Ren, *Appl. Phys. Lett.*, 2016, **109**, 183101.
2. D. Xiang, C. Han, Z. Hu, B. Lei, Y. Liu, L. Wang, W. P. Hu and W. Chen, *Small*, 2015, **11**, 4829-4836.
3. X. Li, H. Zhu, K. Wang, A. Cao, J. Wei, C. Li, Y. Jia, Z. Li, X. Li and D. Wu, *Adv. Mater.*, 2010, **22**, 2743-2748.
4. Q. Dong, Y. Fang, Y. Shao, P. Mulligan, J. Qiu, L. Cao and J. Huang, *Science*, 2015, **347**, 967-970.
5. W. Zhu, C. Zhang, Q. Li, L. Xiong, R. Chen, X. Wan, Z. Wang, W. Chen, Z. Deng and Y. Peng, *Appl. Catal. B-Enviro.*, 2018, **238**, 339-345.
6. H. Li, X. Li, J.-H. Park, L. Tao, K. K. Kim, Y. H. Lee and J.-B. Xu, *Nano Energy*, 2019, **57**, 214-221.

7. X. Liu, F. Li, M. Xu, T. Shen, Z. Yang, W. Fan and J. Qi, *Langmuir*, 2018, **34**, 14151-14157.
8. Z. Liang, P. Zeng, P. Liu, C. Zhao, W. Xie and W. Mai, *ACS Appl. Mater. Interface.*, 2016, **8**, 19158-19167.
9. L. Z. Hao, Y. J. Liu, W. Gao, Z. D. Han, Z. J. Xu, Y. M. Liu and J. Zhu, *RSC Advances*, 2016, **6**, 40192-40198.
10. W. Song, X. Wang, H. Chen, D. Guo, M. Qi, H. Wang, X. Luo, X. Luo, G. Li and S. Li, *J. Mater. Chem. C*, 2017, **5**, 11551-11558.
11. F. Cao, Q. Liao, K. Deng, L. Chen, L. Li and Y. Zhang, *Nano Research*, 2018, **11**, 1722-1730.
12. Y. Zhang, W. Xu, X. Xu, W. Yang, S. Li, J. Chen and X. Fang, *Nanoscale Horizons*, 2019, **4**, 452-456.
13. T. Shen, D. Binks, J. Yuan, G. Cao and J. Tian, *Nanoscale*, 2019, **11**, 9626-9632.
14. Y. Dai, X. Wang, W. Peng, C. Xu, C. Wu, K. Dong, R. Liu and Z. L. Wang, *Adv. Mater.*, 2018, **30**, 1705893.
15. L. Z. Hao, W. Gao, Y. J. Liu, Y. M. Liu, Z. D. Han, Q. Z. Xue and J. Zhu, *Phys. Chem. Chem. Phys.*, 2016, **18**, 1131-1139.
16. Y. Zhang, T. Ji, W. Zhang, G. Guan, Q. Ren, K. Xu, X. Huang, R. Zou and J. Hu, *J. Mater. Chem. C*, 2017, **5**, 12520-12528.
17. P. Joshna, S. R. Gollu, P. M. P. Raj, B. Rao, P. Sahatiya and S. Kundu, *Nanotechnology*, 2019, **30**, 365201.
18. P. Ghamgosar, F. Rigoni, M. G. Kohan, S. You, E. A. Morales, R. Mazzaro, V. Morandi, N. Almqvist, I. Concina and A. Vomiero, *ACS. Appl. Mater. Interfaces*, 2019, **11**, 23454-23462.
19. L. Chen, W. Tian, C. Sun, F. Cao and L. Li, *ACS. Appl. Mater. Interfaces*, 2019, **11**, 3241-3250.
20. C.-C. Cheng, J.-Y. Zhan, Y.-M. Liao, T.-Y. Lin, Y.-P. Hsieh and Y.-F. Chen, *Appl. Phys. Lett.*, 2016, **109**, 053501.
21. M. Kang, S. Yoon, J. Cho, J. Kim and D. S. Chung, *ACS. Appl. Mater. Interfaces*, 2019, **11**, 8365-8373.
22. D. Wu, Y. Jiang, Y. Zhang, Y. Yu, Z. Zhu, X. Lan, F. Li, C. Wu, L. Wang and L. Luo, *J. Mater. Chem.*, 2012, **22**, 23272.
23. C. Y. Wu, Z. Q. Pan, Y. Y. Wang, C. W. Ge, Y. Q. Yu, J. Y. Xu, L. Wang and L. B. Luo, *J. Mater. Chem. C*, 2016, **4**, 10804-10811.
24. E. Mulazimoglu, S. Coskun, M. Gunoven, B. Butun, E. Ozbay, R. Turan and H. E. Unalan, *Appl. Phys. Lett*, 2013, **103**, 083114.
25. A. A. M. Farag, A. Ashery, E. M. A. Ahmed and M. A. Salem, *J. Alloys. Compd*, 2010, **495**, 116-120.
26. P. Chetri and J. C. Dhar, *Sci. Semicon*, 2019, **100**, 123-129.
27. A. I. Nusir, S. J. Bauman, M. S. Marie, J. B. Herzog and M. O. Manasreh, *Appl. Phys. Lett.*, 2017, **111**, 171103.
28. H. Fang, C. Zheng, L. Wu, Y. Li, J. Cai, M. Hu, X. Fang, R. Ma, Q. Wang and H. Wang, *Adv. Funct. Mater.*, 2019, **29**, 1809013.